*Int. J. Electrochem. Sci.*, 16 **(2021)** Article Number: 211240, doi: 10.20964/2021.12.39

International Journal of
ELECTROCHEMICAL
SCIENCE
www.electrochemsci.org

# High-sensitivity $SO_2$ Gas Sensor Based on Noble Metal Doped $WO_3$ Nanomaterials

*Hang Liu, Jiani Zhou, Lanyi Yu, Qiuchen Wang, Bing Liu, Peihua Li, Yuhong Zhang*[*]

School of electrical and computer engineering, Jilin jianzhu university, Changchun 130118, China
[*]E-mail: zhangyuhong@jlju.edu.cn, Liuhang76@163.com

*Received:* 2 September 2021 / *Accepted:* 12 October 2021 / *Published:* 10 November 2021

In this paper, the $WO_3$ nanoparticles(NPs) were prepared by a facile and low cost chemical coprecipitation method. Then the Pt-$WO_3$ and Au-$WO_3$ were synthesized. The morphologies of the samples were represented by XRD and SEM. Sensing characteristics of novel metal doped $WO_3$ sensors were investigated by exposure to $SO_2$ gas at different operating temperature. The sensor response for $SO_2$ gas was measured with different concentrations from 100 ppb to 16 ppm. As a result, the 1 wt%Pt-$WO_3$ sensor presented a greatly low detection limit of 100 ppb at optimum operating temperature of 160 °C. The sensitivity of 1 wt%Pt-$WO_3$ sensor for 100 ppb reached 4.1. As well as a better sensor response as compared to the other $SO_2$ gas sensor. It demonstrated that the Pt-$WO_3$ materials may be used to develop the commercial $SO_2$ gas sensor.

**Keywords:** $SO_2$, $WO_3$ nanoparticles, coprecipitation, Sensing characteristics

## 1. INTRODUCTION

The sulfur dioxide ($SO_2$) is one of the most dangerous air pollutants for environmental and public health. It is produced from burning of oil and coal in power stations, industrial plants and cars. The other sources of $SO_2$ include the volcanic eruptions, forest fires and hot springs. The $SO_2$ gas induces the formation of acid rain, which destroys the ecological environment and affects ecological balance of water and soils. Excessive $SO_2$ exposure will harm the health of eyes, throat and lungs. Generally, the exposure threshold limit of $SO_2$ has been set 5 ppm[1]. Even though the exposure limit in one hour for $SO_2$ only is set 75 ppb based on the US National Ambient Air Quality Standards[2]. Therefore, it is urgent to develop $SO_2$ sensors with excellent and accurate response at low concentration. The traditional $SO_2$ sensors mainly are based on the spectra, acoustic and gas chromatography technologies[3-5]. But the sensors for $SO_2$ detection are complicated and expensive, which inhibit the development in practical

application. The chemical sensors based on the semiconductor metal oxide have the advantages of rapid response, high sensitivity, and low fabrication cost[6-8]. Comparing with other kinds of gas sensors, semiconductor metal oxide gas sensors are very suitable for industrial and safety issues due to their advantages that make the orientation of the researches to develop the sensors detection performance to meet the safety requirements

Over the past few years, semiconductor-based $SO_2$ sensors are reported using various materials such as $In_2O_3$, ZnO, $TiO_2$ and $SnO_2$. Zhou et al. report the gas sensing characteristics of the NiO-ZnO nanodisks materials. The maximum sensitivity reaches 16.25 at 240 °C for $SO_2$ gas[1]. Egdell et al. prepare the V-doped $TiO_2$ materials and measured the sensing characteristics for $SO_2$ gas as low as 10 ppm at 200 ℃[9]. Sen et al. report the sensing characteristics of the $V_2O_5$-doped $SnO_2$ materials for $SO_2$ gas. The low detection limit is 5 ppm at operating temperature 350 ℃[10]. Mulmi et al reported a $SnO_2$-$TiO_2$(S-T) composite sensor. The sensor shows the stable and repeated sensitivities with response time of ~5 mins for 10-40 ppm $SO_2$ in $N_2$ at 450 ℃[11]. Tyagi et al used $SnO_2$ thin films on platinum (Pt) interdigital electrode patterned substrates as the gas sensor. A maximum sensing response of 9 has been obtained for gold catalyst at a relatively low temperature of 60°C for 500 ppm of $SO_2$ gas[12]. Unfortunately, the low detection limit of these gas sensors to $SO_2$ gas is about ~ppm. They are not suitable for detect the ppb level $SO_2$ gas.

Tungsten trioxide ($WO_3$) is one of the n-type metal oxide semiconductors with a wide band gap (2.5-3.0 eV), and various $WO_3$ nanostructures have been developed for sensors including nanowires, nanorods, nanoplates, nanofibers, hollow microspheres and many hierarchical nanostructures[13-17]. Moreover, the sensitive properties of the $WO_3$ materials can be enhanced by loaded and doped novel metals or other metal oxides. The novel metals have been used the catalysis to increase the material porosity. Thus the gas adsorption ability in the specific surface can be increased. In the present study, pure $WO_3$, Pt-$WO_3$ and Au-$WO_3$ nanoparticles are synthesized by a facile and low cost chemical coprecipitation method and their gas sensing responses towards $SO_2$ are investigated. Finally, the possible sensing mechanism of the metal doped $WO_3$ for $SO_2$ gas is also discussed.

## 2. EXPERIMENTAL

### *2.1 Preparation of $WO_3$ Nanoparticles*

The $WO_3$ Nanoparticles were prepared via a chemical co-precipitation method. The chemical reagents were of analytical grade. $Na_2WO_4 \cdot 2H_2O$ was added in the deionized water and obtained the $Na_2WO_4$ solution (as the solution A). Then a certain concentration HCl was dropwise added into the solution A, and continue to stir for 30 minutes to fully react. Finally, the obtained product was completely washed. The deionized water and ethanol were used by alternation. At last, the samples were calcined in an oxygen atmosphere at a temperature of 550 °C for 30 min. The pure $WO_3$ NPs were obtained.

For obtained the Pt-$WO_3$ and Au-$WO_3$ samples, the chloroplatinic acid and chloroauric acid were added the above pure $WO_3$ with definite proportion. Then ground in a mortar for 20 minutes. At last the mixtures were calcined at 550℃ for 30 minutes in the muffle furnace. The x wt% Pt-doped $WO_3$(x=0.5,

1, 1.5) and y wt% Au-doped $WO_3$(y=0.5, 1, 1.5) powers were acquired for the following experiment.

### *2.2 Characterization*

The X-ray diffraction (XRD) shapes of pure $WO_3$, Pt-doped $WO_3$ and Au-doped $WO_3$ were measured from 20° to 60° (2θ degree). The Rigaku Ultima IV X-ray Diffractometer with Cu-Kα radiation (λ=0.15406 nm) was used with a screening rate of 10° $min^{-1}$ (0.02° step). Its working voltage was 40 KV and current was 40 mA. The morphology of the samples was acquired by using FE-SEM, Quanta 450.

### *2.3 Fabrication and measurement of gas sensor*

The traditional heater-type thick film gas sensor was employed in this work. The Fig.1 shown the basic structure of the semiconductor gas sensor. The sensing materials and deionized water were hybrid with a volume ratio. The mixture materials form a homogeneous paste by grinding. The prefabricated ceramic tube with a pair of gold electrodes and platinum wires was brushed manually with the paste to form a sensing film. The Ni-Cr alloy coil was used as a heater. The operating temperature of the sensor was governed by changing the Ni-Cr alloy coil current. All of the sensors were aged at 220 °C for 48 h. The stability and repeatability of the sensor can be improved.

The gas sensing performances were measured the CGS-8 intelligent gas sensing analysis system (Beijing Elite Tech Co. Ltd., China). The $SO_2$ gas was loaded into the solid cylinder by a syringe. First the sensor was exposed on the air. Then the sensor was exposed to the test gas for some moment when the value of the sensor resistance became stable. The sensor response (S) was well-defined as:

$$S = R_{air}/R_{gas} \quad (1)$$

where $R_{gas}$ was the resistance of the gas sensor in the test gas. $R_{air}$ was the resistance of the gas sensor in air. The response time was defined the time which was required to reach its minimum resistance in the exposure of test gas. While the recovery time was defined the time which was required to recuperate higher than 90% of its initial resistance in the air.

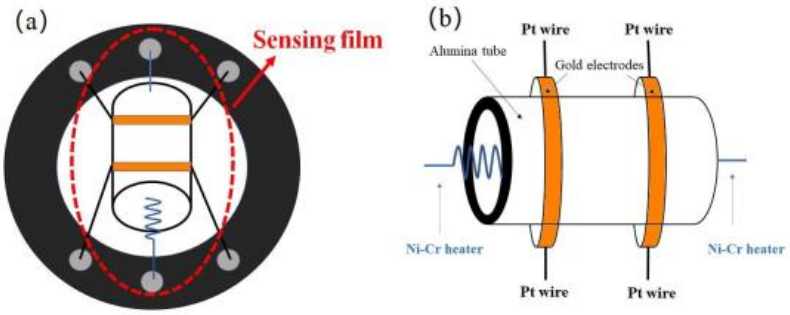


**Figure 1.** (a) A complete side-heated gas sensor (b) The structure diagram of a ceramic tube coated with sensitive materials

## 3. RESULTS AND DISCUSSION

### *3.1. Materials characterization*

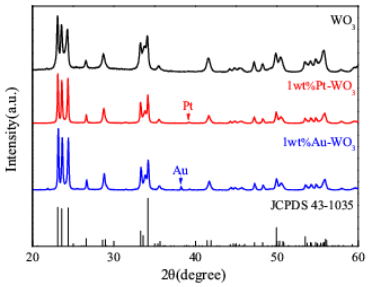


**Figure 2.** Typical XRD pattern of prepared $WO_3$, 1wt%Au-$WO_3$ and 1wt%Pt-$WO_3$ nanoparticles.

Fig.2 represents the typical XRD spectrum for the pure $WO_3$ and 1wt%Pt-$WO_3$ , well-defined diffraction peaks at 23.12° , 23.59° , 24.38° , 26.59° , 28.94° , 33.27° , 34.16° , 41.91° , 47.26° , 48.25° , 49.77° , 56.11° correspond to (002) , (020) , (200) , (120) , (112) , (022) , (202) , (222) , (004) , (040) , (041) and (402) diffraction planes of the $WO_3$ structure, respectively. Compared with the JCPDS no. 43-1035, the peaks of the samples are in good agreement with the standard card. The sharp peaks suggest that the crystallinity of $WO_3$ material is perfect. When the 1wt%Au and 1 wt%Pt were doped into the $WO_3$ host, the weak diffraction peak of Au and Pt could be observed. It proves that the Au and Pt are doped effectively in the host.

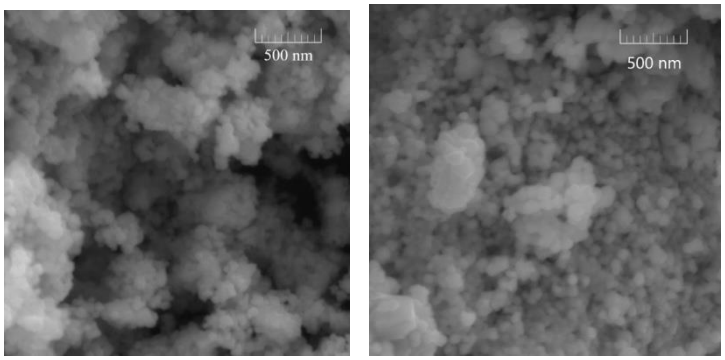


**Figure 3.** (a)SEM images of the $WO_3$ samples (b) SEM images of the 1wt%Au-$WO_3$ samples

The morphology of the pure $WO_3$ and Au doped $WO_3$ samples are presented through the SEM images. As shown in Fig.3. All of the samples present the nanoscale. The size of the $WO_3$ sanmples is about 50 nm. It is well identified and aggregated with the nanoparticles. And the size of the particles is almost uniform.

### *3.2 Sensing characterization*

#### *3.2.1 Gas sensing characteristics of $WO_3$ and Pt-$WO_3$ nanomaterials*

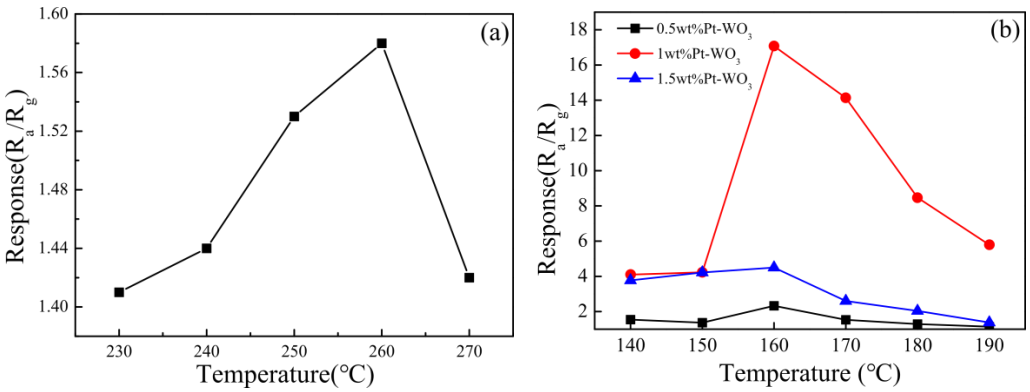


**Figure 4.** (a)The gas response of the pure $WO_3$ nanoparticles based sensor to 8 ppm of $SO_2$ gas at different operating temperatures (b) The gas response of the x wt%Pt-$WO_3$(x=0.5, 1, 1.5) nanoparticles based sensor to 8 ppm of $SO_2$ gas at different operating temperatures

It is well known that sensitivity, operating temperature, response/recovery time play very crucial roles in the gas sensor. The gas sensitive performances of pure $WO_3$ and Pt-doped $WO_3$ are tested. As shown in Fig.4(a), the response of the pure $WO_3$ sensor to 8 ppm $SO_2$ varies with the operating temperature are illustrated from 230 ℃ to 270 ℃. The response values increased first and decreased sharply.

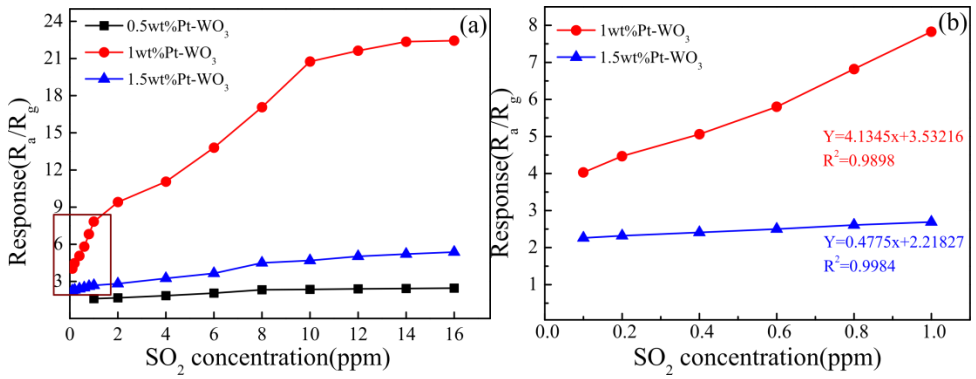


**Figure 5** (a) Responses of the Pt-$WO_3$ sensors vs $SO_2$ concentrations at 160°C (b) Responses of the Pt-$WO_3$ sensors at the concentration from 100 ppb to 1 ppm.

The maximum response of the pure $WO_3$ sensor is lower, which reaches 1.58 at 260 ℃. However, the response values of the sensors could be enhanced with the Pt was doped into the $WO_3$. Fig.4(b) presents the responses of the Pt-doped $WO_3$ sensors for 8 ppm $SO_2$. The response enhances with the increase of the Pt concentration, which it reaches the maximum at the 1%Pt-$WO_3$. The maximum response appeared at its optimum operating temperature (160 ℃) was 17.07. Notably, the optimal operating temperature of all the Pt-$WO_3$ sensors are about lower 100 ℃ than that of pure $WO_3$ sensor.

This operating temperature also is lower than most other gas sensor based on $WO_3$ materials[18-20]. The 1wt%Pt-$WO_3$ nanoparticles exhibited about 10.8 times enhancement in gas response to 8 ppm $SO_2$ in comparison to pure $WO_3$ nano-particles. The results indicate that the gas sensing response of the Pt-$WO_3$ nanoparticles is significantly improved due to the introduction of Pt. Comparing with the pure $WO_3$, the operating temperature of Pt-$WO_3$ material also decreases. The enhancement in the sensitive performances of Pt-$WO_3$ samples is mainly due to the catalytic efficiency of Pt.

Fig.5a shown the responses of the Pt-$WO_3$ sensors toward $SO_2$ concentrations ranging from 100 ppb to 16 ppm at 260 °C. The response values of the 1 wt%Pt-$WO_3$ sensor for different concentration $SO_2$ gas is higher than that of the other two. And the response values of these sensors improve linearly with the increasing of the $SO_2$ gas concentration. The saturation phenomenon of the gas response also presents when the gas concentration is over 10 ppm. The sensor response value of the 1%Pt-$WO_3$ sensor to 100 ppb $SO_2$ gas is 4.2. The detection limits of 1 wt%Pt-$WO_3$ sensor for $SO_2$ are lower than that of some other reported results[21-23]. Furthermore, the gradient of the $SO_2$ gas sensor response in the range of 100 ppb–1 ppm is higher than that of over 1 ppm, which reveales that the Pt-$WO_3$ sensor has the widest linear range for detecting the ppb level $SO_2$. It indicates that the Pt-$WO_3$ sensors can satisfy the application for monitoring $SO_2$ gas, especially of ppb level gas concentrations. The response values of the 1 wt%Pt-$WO_3$ and 1.5 wt%Pt-$WO_3$ sensors are presented at the $SO_2$ gas concentration from 100 to 1000 ppb. The linear fitting equations for the 1 wt%Pt-$WO_3$ and 1.5 wt%Pt-$WO_3$ gas sensors are $y=4.1345\ x+3.53216$, $R^2=0.9898$ and $y=0.4775\ x+2.21827$, $R^2=0.9984$, respectively. Where y is the gas response and *x* is the concentration of the detecting gas. The 1 wt%Pt-$WO_3$ gas sensor for $SO_2$ shows the highest slope of 4.1345. The sensitivity increased linearly with the $SO_2$ concentration with R-square confidence value above ~0.90 and the response was fitted, and it was found that the response value and the concentration showed a good linear relationship. The outstanding linearity can decrease the measurement error in the concentration range from 100 to 1000 ppb.

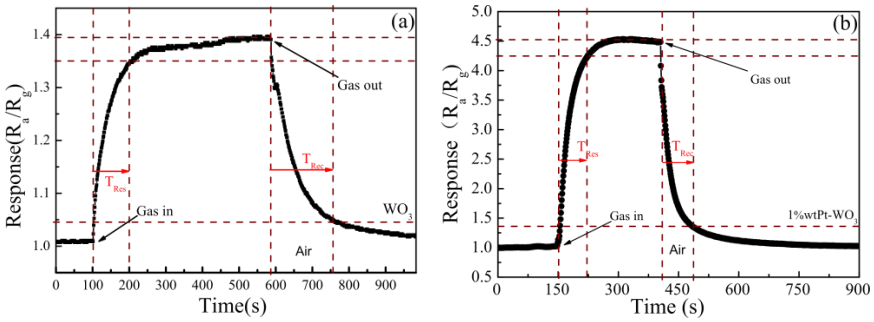


**Figure 6.** (a) Response and recovery curves of the pure $WO_3$ $SO_2$ sensor for 8 ppm gas (b) Response and recovery curves of 1 wt%Pt-$WO_3$ $SO_2$ sensor for 100 ppb gas

Both response and recovery times are important parameters of gas sensors used for real-time detection. In this paper, the transient response curves of the pure $WO_3$ and 1 wt%Pt-$WO_3$ sensors have been investigated and displayed in Fig.6. It can be obtained that the response/recovery times for pure $WO_3$ materials are 300 and 85 s for 8 ppm $SO_2$ at 260 ℃, respectively. While the response/recovery times of 1 wt%Pt-$WO_3$ sensor reach 150/200 s for 100 ppb $SO_2$ at 160 ℃, respectively. Obviously, Pt

doped in $WO_3$ host can enhance the response time than that of pure $WO_3$. The higher response value and faster response time are mainly induced by Pt's catalytic effect. The activation energy of the surface reaction can be decreased by the Pt's catalytic effect. So the redox reaction process is accelerated. Then the response time become small.

### *3.2.2 Gas sensing characteristics of Au-$WO_3$ nanomaterials*

In this paper, the sensitivities Au-$WO_3$ sensor are also investigated. Fig.7(a) presents the responses of the Au-doped $WO_3$ sensors for 8 ppm $SO_2$. The response of 1 wt%Au-$WO_3$ sensor reaches 2.6 at an operating temperature of 290 ℃. The maximum response is enhanced 1.65 times than the reference sample (pure $WO_3$). It indicates that the response values of the Au-$WO_3$ sensor for $SO_2$ gas are higher than the pure $WO_3$ sensors. The response values of the Au-$WO_3$ sensors at different concentration $SO_2$ gas have been shown in Fig.7(b). The response values of the Au-$WO_3$ sensors for $SO_2$ gas indicate almost linear increasing with the gas concentration increasing, and the slope changes slowly when the $SO_2$ concentrations exceed 12 ppm.

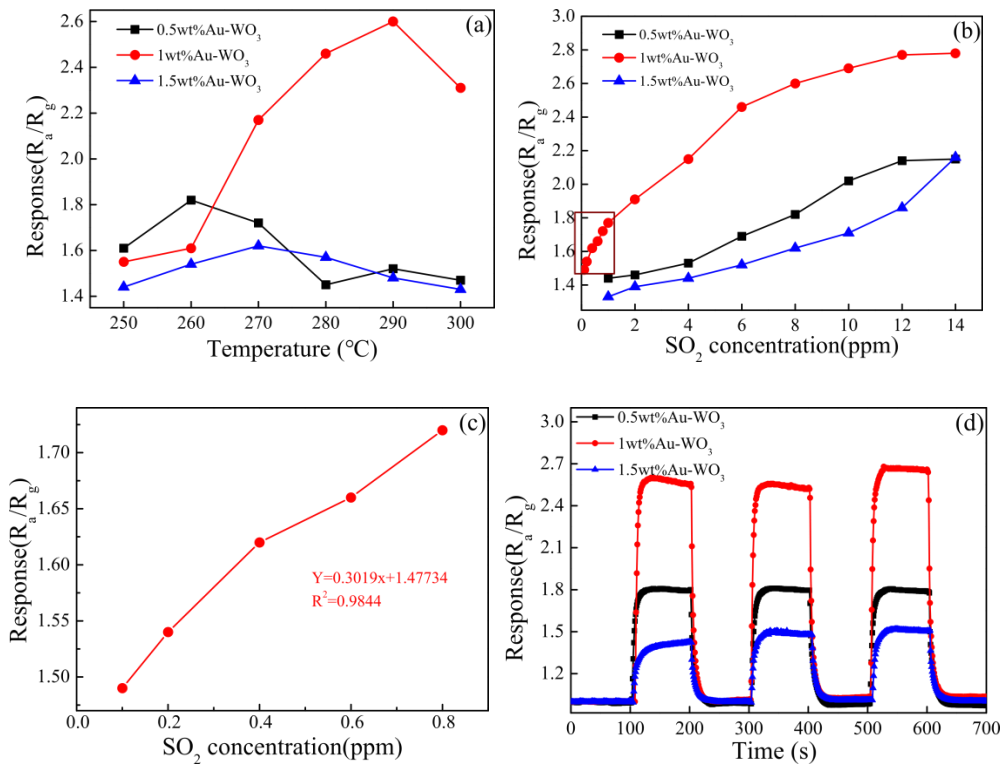


**Figure 7.** (a) Responses of the Au-$WO_3$ sensors vs operating temperature to 8 ppm $SO_2$. (b) Responses of the Au-$WO_3$ sensors vs $SO_2$ concentrations at 290 °C. (c)Responses of the 1 at%Au-$WO_3$ sensors from 100 ppb to 1 ppm. (d) Transients curve of Au-$WO_3$ sensors to 8 ppm $SO_2$.

The Saturation phenomenon begins to appear for detecting $SO_2$ gas. Fig.7c shows the response (S) of the 1%Au-$WO_3$ sensors for 100 ppb to 1 ppm $SO_2$. The linear fitting equations for the 1% Au-

$WO_3$ and gas sensors were Y=0.3019x+1.47734, $R^2$=0.9844. It was found that the response value and the concentration showed a good linear relationship. The stability of the Au-$WO_3$ sensor is investigated through three consecutive exposures for 8 ppm $SO_2$, as shown in Fig. 7(d). The sensor responses change slightly, and the respond and recovery times also keep stable basically. It demonstrates that the Au-$WO_3$ sensor have a good for detecting $SO_2$ gas. The response time of 1 wt%Au-$WO_3$ sensor is 10 s, and the recovery time is 20 s. Compared with the pure $WO_3$ sensor, the response time of 1wt% Au-$WO_3$ sensor is shortened by 30 times and the recovery time is shortened by 5.6 times. In addition, Au doped samples can alleviate the baseline resistance drift during $SO_2$ testing, so the thermal stability of this group of samples is better than that of pure $WO_3$ sensor.

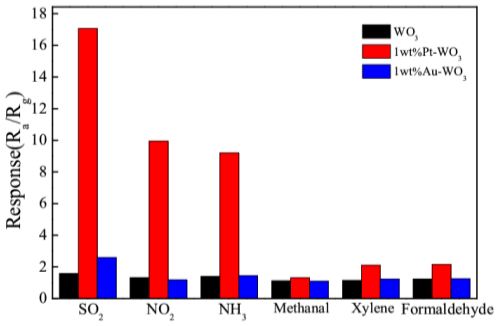


**Figure 8.** Selectivity of the $WO_3$, Pt-$WO_3$ and Au-$WO_3$ sensors to the gases tested.

**Table 1.** Responses of different nanomaterials to $SO_2$ gas.

| Material | Temperature(℃) | Concentration | Response | $t_{rea}/t_{rec}$ | limit of detection | Ref |
|---|---|---|---|---|---|---|
| Pt-$WO_3$ | 160 | 8 ppm | 17.07 | 150 s/200 s | 100 ppb | this work |
| Au-$WO_3$ | 290 | 8 ppm | 2.6 | 10 s/20 s | 100 ppb | this work |
| NiO-ZnO | 240 | 20 ppm | 16.25 | 52 s/41 s | 5 ppm | [1] |
| $SnO_2$-$TiO_2$ | 450 | 100 ppm | 11.5 | 5 min/- | 10 ppm | [11] |
| Au-$SnO_2$ | 60 | 500 ppm | 9 | 280 s/300 s | 500 ppm | [12] |
| $WO_3$ FET | 150 | 125 ppm | 22.82%$R_a$ | 140 s/360 s | 10 ppm | [17] |
| $TiO_2$ nanoplate | 200 | 10 ppm | 3.3 | 18 s/- | 1 ppm | [24] |
| RGO/$WO_3$ | 25 | 100 ppb | 1.17 | 66 s/298 s | 30 ppb | [25] |
| NiO/$SnO_2$ | 180 | 500 ppm | 56 | 80 s/70 s | 5 ppm | [26] |
| Ni-$MoS_2$ | RT | 5 ppm | 7.4%$R_a$ | 50 s/56 s | 250 ppb | [27] |
| CuO | 200 | 10 ppm | 2.8 | 15 s/220 s | 1 ppm | [28] |
| Ru/$Al_2O_3$/ZnO | 350 | 5 ppm | 1.15 | 1 min/6 min | 5 ppm | [29] |
| AuNPs-$SnO_{2-x}$ | 200 | 20 ppm | 10.43 | 34 s/14 s | 500 ppb | [30] |
| RGO-$SnO_2$ | 60 | 500 ppm | 22 | 2.4 min/3.5 min | 10 ppm | [31] |
| $SnO_2$ dodecahedrons | 183 | 10 ppm | 1.92 | 200 s/- | 400 ppb | [32] |

Table 1 summarizes the sensing performances of some $SO_2$ gas sensor. The sensing properties of the Pt-$WO_3$ and Au-$WO_3$ sensors are compared by other sensors reported in the literature for detecting $SO_2$ gas. The Pt-$WO_3$ $SO_2$ sensor shows the lowest detection limit(100 ppb), short response/recovery times(150/200 s) and lower operating temperature(160 °C). The comparing results confirm that the Pt-$WO_3$ $SO_2$ sensors are prior to some other sensors.

At last, the selectivity of the $WO_3$, Pt-$WO_3$ and Au-$WO_3$ sensors with the highest sensitivity is tested. Fig. 8 shows the results of the selectivity for different gas at their optimal operating temperature. Under the same conditions, the working temperature is 160℃ and the detection concentration is 8 ppm. It is clear that the higher selectivity is reached at the 1 wt% Pt-$WO_3$ sensors. As a result, the Pt-doped $WO_3$ sensor is a very promising semiconductor to monitor $SO_2$ at relatively low temperature; both sensitivity and selectivity are taken into consideration.

### *3.3. Gas sensing mechanism*

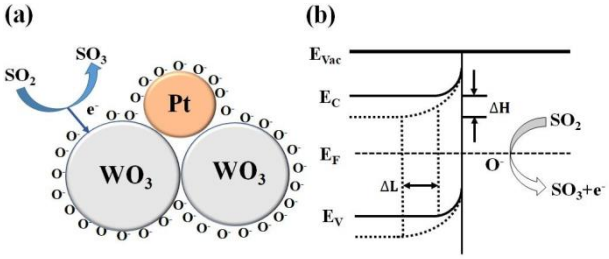


**Figure 9.** (a) Schematic view of possible gas sensing mechanisms: catalytic reactions between target $SO_2$ and oxygen adsorbates releasing electrons back into the Pt-$WO_3$ surface. (b) Schematic energy band diagram of Pt-$WO_3$ NPs

Therefore, the $SO_2$ gas sensing mechanism of the sensors developed herein can be discussed based on the reports of Gupta et al.[26]. The $WO_3$ gas sensitive material belongs to the n-type metal oxide semiconductor. The oxygen molecules are adsorbed on the $WO_3$ grains and their grain boundaries in the air. The electrons from conduction band of the $WO_3$ are pull out, which results in the formation of oxygen ions ($O_2^-$, $O^-$ and $O^{2-}$) adsorbed at the surface of $WO_3$.

$O_{2(gas)}+2e^-\rightarrow 2O^-_{(ads)}$

$SO_2$ is reducing gas. When the $WO_3$ sensor is placed into the $SO_2$ gas, the reaction process will occur on the surface of $WO_3$. $SO_2+O^-\rightarrow SO_3+e^-$, Some electrons become free electrons from the adsorbed oxygen ions, then return to the conduction band. The height of the grain boundary barrier decreases and the electron mobility increases, which reduce the sensor's resistance. As is known that the gas sensing properties of semiconductor gas sensors can be enhanced by doped noble metals. In this paper, the Pt and Au catalysts are used to improve the gas sensing properties of semiconductor gas sensors. Such as with Pt loading, the Pt nanoparticles can either form a solid solution by replacing the host atom in the crystal lattice or exist in the form of interstitial space in the host crystal lattice, which will form Schottky junctions with $WO_3$ nanoparticles leading to additional local extension of depletion regions. The doped

Pt also have higher electron affinity, which makes the increase of electron concentration larger and the change of electrical resistance more significant. So the sensitivity and selectivity of the sensors are enhanced.

## 4. CONCLUSION

In summary, the pure $WO_3$ nanoparticles are synthesized by chemical coprecipitation method, and Pt-$WO_3$ and Au-$WO_3$ samples are prepared by impregnation method. The microstructures of the samples are characterized by XRD and SEM, and it is confirmed that the prepared samples are nanoparticles. Gas sensing characterization tests are performed on all sensors. Among them, the 1 wt%Pt-$WO_3$ content sample has lowest detection limit (100 ppb with $R_{air}/R_{gas}$ = 4.1 at 160 ℃). The 1 wt%Au-$WO_3$ content sample has the fastest response/recovery time(10 s/20 s toward 8 ppm at 290 ℃). In brief, the novel metals (Pt and Au) play an important role for enhancing the sensing performances of the pure $WO_3$. The lower operating temperature, higher response value and lower detection limit are obtained. Therefore, the $WO_3$ materials with doped into proper concentration Pt or Au nanoparticles are proposed to become a candidate for a $SO_2$ sensor with high response, low detection limit.

ACKNOWLEDGMENTS
This work was supported by Natural Science Foundation of China (Grant No:61705077); Science Foundation of Jilin Province Education Department (JJKH20190853KJ); Project of Jilin Provincial Science and Technology Department (No:20190303064SF, 20200403072SF); Project of Jilin Province Development and Reform Commission (2019C048-4, 2020C021-5).

## References

1. Q. Zhou, W. Zeng, W.G. Chen, L.N. Xu, R. Kumar and A. Umar, *Sensors and Actuators, B: Chemical*, 298 (2019) 126870.
2. https://www.epa.gov/criteria-air-pollutants/naaqs-table#4.
3. M.A. Gondal and J. Mastromarino, *Applied Optics*, 40 (2001) 2010.
4. H.Y. Xu, K.M. Wang, D.N. Wang and Q.C. Li, *Chemical Research in Chinese Universities*, 19 (1998) 1401.
5. M. Nonomuraac and T. Hobob, *Journal of Chromatography A*, 804 (1998) 151.
6. A. Dey, *Materials Science & Engineering B: Solid-State Materials for Advanced Technology*, 229 (2018) 206.
7. A. Mirzaei, S.G. Leonardi and G. Neri, *Ceramics International*, 42 (2016) 15119.
8. J.H. Lee, *Sensors and Actuators, B: Chemical*, 140 (2009) 319.
9. D. Morris and R.G. Egdell, *Journal of Materials Chemistry C*, 11 (2001) 3207.
10. S. Das, S. Chakraborty, O. Parkash, D. Kumar, S. Bandyopadhyay, S.K. Samudrala, A. Sen and H.S. Maiti, *Talanta*, 75 (2008) 385.
11. S. Mulmi and V. Thangadurai, *Ionics*, 22 (2016) 1927.
12. P. Tyagi, A. Sharma, M. Tomar and V. Gupta, *Emerging Materials Research*, 6 (2017) 3.
13. G. Adilakshmi, R. Subba Reddy, A. Sivasankar Reddy, P. Sreedhara Reddy and Ch. Seshendra Reddy, *Journal of Materials Science: Materials in Electronics*, 31 (2020) 12158.

14. T. Samerjai, N. Tamaekong, C. Liewhiran, A. Wisitsoraat and S. Phanichphant, *Journal of Solid State Chemistry*, 214 (2014) 47.
15. H.J. Xia, Y. Wang, F.H. Kong, S.R. Wang, B.L. Zhu, X.Z. Guo, J. Zhang, Y.M. Wang and S.H. Wu, *Sensors and Actuators, B: Chemical*, 134 (2008) 133.
16. Z.J. Han, J. Rena, J.J Zhou, S.Y Zhang, Z.L. Zhang, L. Yang, and C.B. Yin, *International Journal of Hydrogen Energy*, 45 (2020) 7223.
17. G. Jung, Y. Jeong, Y. Hong, M. Wu, S. Hong, W. Shin, J. Park, D. Jang and J.H. Lee, *Solid State Electronics*, 165 (2020) 107747.
18. R.J. Bose, N. Illyaskutty, K.S . Tan, R.S. Rawat, M.V. Matham, H. Kohler and V.P.M. Pillai, *Europhysics Letters*, 114 (2016) 66002.
19. X.H. Liu, J. Zhang, T.L. Yang, X.Z. Guo, S.H. Wu and S.R. Wang, *Sensors and Actuators, B: Chemical*, 156 (2011) 918.
20. X.J. Yang, V. Salles; Y. V. Kaneti, M. Liu; M. Maillard, C. Journet, X.C. Jiang and A. Brioude, *Sensors and Actuators, B: Chemical*, 220 (2015) 1112.
21. D.Z. Zhang,M.S. Pang, J.F Wu and Y.H. Cao, *New Journal of Chemistry*, 43 (2019) 4900.
22. S.C. Lee, B.W. Hwang, S.J. Lee, H.Y. Choi, S.Y. Kim, S.Y. Jung, D. Ragupathy, D.D. Lee and J.C. Kim, *Sensors and Actuators, B: Chemical*, 160 (2011) 1328.
23. D.W. Shin, T.M. Besmann and B.L. Armstrong, *Sensors and Actuators, B: Chemical*, 176 (2013) 75.
24. W. Guo, Q.Q. Feng, Y.F. Tao, L. J. Zheng, Z.Y. Han and J.M. Ma, *Materials Research Bulletin*, 73 (2016) 302.
25. P.G. Su and Y.L. Zheng, *Analytical Methods*, 13 (2021) 782.
26. P. Tyagi, A. Sharma, M. Tomar and V. Gupta, *Sensors and Actuators, B: Chemical*, 224 (2016) 282.
27. D.Z. Zhang, J.F. Wu, P. Li and Y.H. Cao, *Journal of Materials Chemistry A*, 5 (2017) 20666.
28. P.V. Tong, N.D. Hoa, H.T. Nha, N.V. Duy, C.M. Hung and N.V. Hieu, *Journal of Electronic Materials*, 47 (2018) 7170.
29. Y.Y Liu, X.Y Xu, Y. Chen, Y. Zhang, X.H. Gao, P.C. Xu, X.X. Li, J.H. Fanga, W.J. Wen, *Sensors and Actuators, B: Chemical*, 262 (2018) 26.
30. L.Y. Liu, and S.T. Liu, *ACS Sustainable Chemistry & Engineering*, 6 (2018) 13427.
31. P. Tyagi, A. Sharma, M. Tomar and V. Gupta, *Sensors and Actuators, B: Chemical*, 248 (2017) 980.
32. X.H. Ma, Q.X. Qin, N. Zhang, C. Chen, X. Liu, Y. Chen, C.N. Lia and S.P. Ruan, *Journal of Alloys and Compounds*, 723 (2017) 595.